A PRECISE DETERMINATION OF THE W AND Z MASSES AT THE CERN $\bar{p}p$ COLLIDER

UA2 Collaboration

Bern–Cambridge–CERN–Heidelberg–Milano–Orsay (LAL)–Pavia–Perugia–Pisa–Saclay (CEN)

J. ALITTI [a], R. ANSARI [b], R.E. ANSORGE [c], D. AUTIERO [d], P. BAGNAIA [e,1], P. BAREYRE [a], G. BLAYLOCK [c], P. BONAMY [a], M. BONESINI [f,e], C.N. BOOTH [c], K. BORER [g], D. BUSKULIC [b], G. CARBONI [d], D. CAVALLI [f], V. CAVASINNI [d], P. CENCI [h], J.C. CHOLLET [b], A.G. CLARK [e], C. CONTA [i], G. COSTA [f], F. COSTANTINI [d,e], J. CRITTENDEN [a], A. DELL'ACQUA [i], B. DE LOTTO [i,2], T. DEL PRETE [d], R.S. DE WOLF [c], L. DI LELLA [e], G.F. EGAN [e,3], K.F. EINSWEILER [e], L. FAYARD [b], A. FEDERSPIEL [g], R. FERRARI [i], M. FRATERNALI [i,4], D. FROIDEVAUX [h], G. FUMAGALLI [e,i], J.M. GAILLARD [b], F. GIANOTTI [f], O. GILDEMEISTER [e], C. GÖSSLING [e,5], V.G. GOGGI [i,e], S. GRÜNENDAHL [j], J.R. HANSEN [e], K. HARA [g,6], S. HELLMAN [e], E. HUGENTOBLER [g], K. HULTQVIST [e], E. IACOPINI [d,7], J. INCANDELA [e], K. JAKOBS [e], P. JENNI [e], E.E. KLUGE [j], N. KURZ [j], S. LAMI [j,d], P. LARICCIA [h], M. LEFEBVRE [e,e], L. LINSSEN [e], M. LIVAN [i,8], P. LUBRANO [e], C. MAGNEVILLE [a], L.MANDELLI [f], L. MAPELLI [e], M. MAZZANTI [f], K. MEIER [e], B. MERKEL [b], J.P. MEYER [a], M. MONIEZ [b], R. MONING [g], M. MORGANTI [d,9], L. MÜLLER [g], D.J. MUNDAY [e], C. ONIONS [e], T. PAL [e,g], M.A. PARKER [e], G. PARROUR [b], F. PASTORE [i], E. PENNACCHIO [i], J.M. PENTNEY [e], M. PEPE [h], L. PERINI [f,4], C. PETRIDOU [d], P. PETROFF [b], H. PLOTHOW-BESCH [j], G. POLESELLO [f,e], A. POPPLETON [e], M. PRIMAVERA [d,10], L. RASMUSSEN [e], J.P. REPELLIN [b], A. RIMOLDI [i], J.G. RUSHBROOKE [e,11], P. SCAMPOLI [h], J. SCHACHER [g], S.L. SINGH [e], S. STAPNES [e], A.V. STIRLING [a], S.N. TOVEY [d,3], G. UNAL [b], M. VALDATA-NAPPI [d,10], V. VERCESI [e,i], A.R. WEIDBERG [e], P.S. WELLS [e], T.O. WHITE [e], D.R. WOOD [d], S.A. WOTTON [e] and H. ZACCONE [a]

[a] *Centre d'Etudes Nucléaires de Saclay, F-91191 Gif-sur-Yvette Cedex, France*
[b] *Laboratoire de l'Accélérateur Linéaire, Université de Paris-Sud, F-91405 Orsay, France*
[c] *Cavendish Laboratory, University of Cambridge, Cambridge CB3 0HE, UK*
[d] *Dipartimento di Fisica dell'Università di Pisa and INFN, Sezione di Pisa, Via Livornese, S. Piero a Grado, I-56100 Pisa, Italy*
[e] *CERN, CH-1211 Geneva 23, Switzerland*
[f] *Dipartimento di Fisica dell'Università di Milano and INFN, Sezione di Milano, I-20133 Milan, Italy*
[g] *Laboratorium für Hochenergiephysik, Universität Bern, Sidlerstraße 5, CH-3012 Bern, Switzerland*
[h] *Dipartimento di Fisica dell'Università di Perugia and INFN, Sezione di Perugia, via Pascoli, I-06100 Perugia, Italy*
[i] *Dipartimento di Fisica Nucleare e Teorica, Università di Pavia and INFN, Sezione di Pavia, Via Bassi 6, I-27100 Pavia, Italy*
[j] *Institut für Hochenergiephysik der Universität Heidelberg, Schröderstraße 90, D-6900 Heidelberg, FRG*

Received 19 February 1990

The UA2 experiment has collected large samples of W and Z events during recent runs at the CERN $\bar{p}p$ Collider at $\sqrt{s}=630$ GeV. These samples have been used to perform precise measurements of the masses of the W and Z bosons. After a careful analysis of systematic errors, an improved result is obtained for the mass ratio m_W/m_Z. This provides a new value for the weak mixing parameter $\sin^2\theta_w$. Furthermore, it can be combined with recent measurements of the Z mass from e^+e^- colliders to give an absolute measurement of the W mass, leading to the result $m_W=80.49\pm0.43(\text{stat})\pm0.24(\text{syst})$ GeV.

1. Introduction

Since the first observation of W and Z bosons at the CERN $\bar{p}p$ Collider [1], their properties have been the subject of intensive study. Recent results from e^+e^- colliders [2] have substantially improved our knowledge of the mass and width of the Z boson, but for measurements of the mass and width of the W boson, it is still necessary to rely on hadron colliders. Unlike the situation in e^+e^- colliders, where the accelerator itself provides a precise calibration of the mass scale, in hadron colliders the decay products of the W and Z must be used to reconstruct their masses. This restricts a precision measurement to leptonic decay modes, and poses a particular challenge owing to the complex environment and small observable cross sections. In a non-magnetic detector such as UA2, the mass scale is derived from the calorimeter calibrations, and many systematic uncertainties cancel when the ratio of the W and Z masses is computed. This ratio, when combined with e^+e^- results for the Z mass, provides a direct test of the standard model, and is the focus of this paper.

The upgraded UA2 detector has recently completed two runs at the CERN $\bar{p}p$ Collider at a center of mass energy of 630 GeV. Successful operation of the antiproton accumulator complex (AAC) and the SPS provided peak luminosities of up to 3×10^{30} $cm^{-2}s^{-1}$. Large samples of $W\to e\nu$ and $Z\to e^+e^-$ decays have been isolated from these data, corresponding to an integrated luminosity of 7.4 pb^{-1}. These samples have been analyzed with the aim of significantly improving our knowledge of the ratio of the W and Z masses.

2. The UA2 detector

The UA2 detector, consisting of central and forward tracking systems surrounded by electromagnetic and hadronic calorimetry, was upgraded during the period 1985 to 1987. Details of the construction and performance of the various detector elements can be found in the references given below.

The central tracking detector contains two arrays of silicon counters (SI) at radii of 3.5 cm and 14.5 cm, which are used for tracking and ionization measurements [3]. Between these two layers, there is a cylindrical drift chamber (JVD) [4]. Immediately outside the silicon arrays, there are two transition radiation detectors (TRD), followed by a scintillating fiber detector (SFD) [5] consisting of fibers arranged into 18 tracking layers followed by a 1.5 radiation length (RL) thick lead converter and a further 6 layers which are used to localize electromagnetic showers initiated in the converter (preshower detector).

The forward tracking detector consists of proportional tubes (ECPT) [6], covering the pseudorapidity range $1.1<|\eta|<1.6$. These tubes are arranged into 6 tracking layers followed by a 2 RL lead converter and a further 3 layers of tubes acting as a preshower detector.

The UA2 central calorimeter [7], which has been modified to accommodate the improved central tracking detectors, covers the pseudorapidity region $|\eta|\leq 1.0$. Each of the 240 cells is longitudinally segmented into an electromagnetic compartment and two hadronic compartments. The new endcap calorimeters [8], consisting of 384 cells in total, are longitudinally segmented into an electromagnetic and a hadronic compartment. The hadronic calorimetry is hermetic down to 5° from the beam axis ($|\eta|=3$), whereas the electromagnetic calorimetry extends to $|\eta|=2.5$. Both systems have a granularity of approximately $\Delta\phi\times\Delta\eta=15^\circ\times0.2$. The response of the calorimeter to hadronic showers depends on the frac-

[1] Present address: Dipartimento di Fisica, Università di Roma, I-00185 Rome, Italy.
[2] Present address: Dipartimento di Fisica, Università di Udine, I-33100 Udine, Italy.
[3] Visitor from the University of Melbourne, Parkville, Victoria 3052, Australia.
[4] Present address: Dipartimento di Fisica, Università di Palermo, I-90133 Palermo, Italy.
[5] Present address: Institut für Physik, Universität Dortmund, D-4600 Dortmund, FRG.
[6] Present address: University of Tsukuba, Tsukuba, Ibaraki 305, Japan.
[7] Also at Scuola Normale Superiore, I-56100 Pisa, Italy.
[8] Present address: Dipartimento di Fisica, Università di Cagliari, I-09100 Cagliari, Italy.
[9] Present address: Dipartimento di Fisica e INFN, Sezione di Bologna, Università di Bologna, I-40126 Bologna, Italy.
[10] Present address: Dipartimento di Fisica dell'Università della Calabria, Cosenza, Italy.
[11] Present address: Bond University, Gold Coast QLD 4217, Australia.

tion of the energy carried by photons in the shower, requiring corrections factors for each compartment to compensate for the different average responses. The electromagnetic compartments were weighted by a factor of 1.18 for the central calorimeter, and by a factor of 1.20 for the endcaps. A factor of 1.06 was also applied to the second hadronic compartment in the central calorimeter to account for leakage through the back of the calorimeter.

These calorimeters have been extensively studied in test beams of muons, pions, and electrons during the period 1986 to 1989. Approximately 25×10^6 events have been collected during this effort to understand the calorimeter response. Initially, all cells of the calorimeters were placed in the test beam to provide an absolute calibration. This energy scale has been tracked using periodic ^{60}Co source and pulser calibrations. Each year, a portion of the calorimeter has been recalibrated in the test beam to verify this procedure, leading to an estimated error of 1% on the energy scale for the electromagnetic calorimetry. Careful studies were performed on a small number of representative cells in order to parametrize the energy scale for electrons as a function of the incident particle direction and impact point. The observed variations are of the order of $\pm 10\%$, and have been accurately modeled by a parametrization of the test beam data which includes the effects of the average energy loss in the preshower detectors [8].

3. Electron and neutrino identification

3.1. Electron measurement

The electron candidates must pass a series of loose trigger requirements before the events are recorded. These requirements were implemented in a three level trigger system, based on information from the calorimeters [9]. The first level used analog sums of the signals from the photomultipliers of the calorimeter cell compartments with $|\eta| \leqslant 2$. At the second level, electron and jet clusters were reconstructed in a special purpose processor using information from a fast digitization of the calorimeter cell signals. A complete calorimeter reconstruction was performed in the third level using the final digitization and a full set of calibration constants. Information on the radius (transverse size) and energy leakage into the hadronic compartments (longitudinal depth) for calorimeter clusters was used to reject backgrounds. Two triggers were used for this study: a single electron trigger which was fully efficient for $P_T(e) \geqslant 12$ GeV, and a two electron trigger which was efficient for $P_T(e) \geqslant 6$ GeV.

The directions of the charged tracks and the position of the event vertex along the beam axis were reconstructed using the SFD and ECPT detectors in conjunction with the SI and JVD detectors. The event vertex was required to lie within 250 mm of the center of the detector, ensuring an accurate reconstruction of the electron direction and energy.

The tracking and preshower sections of the SFD were used to match the trajectories of candidate central electron tracks with the position of electromagnetic showers with a resolution, measured using electrons from $W\rightarrow e\nu$ decays, of $\sigma_{r\phi}=0.4$ mm in the r–ϕ plane (perpendicular to the beam axis) and $\sigma_z=1.1$ mm along the beam direction. The quality of a track-preshower match was defined by the variable $d_\sigma^2 = (\Delta_{r\phi}/\sigma_{r\phi})^2+(\Delta_z/\sigma_z)^2$ where $\Delta_{r\phi}$ and Δ_z are the measured displacements between the track and preshower positions. Accidental overlaps between photon showers and charged tracks give large values of d_σ^2, and candidate electrons were required to have $d_\sigma^2<25$. In the forward regions, the resolution was 5 mm in both orthogonal directions, and candidates were required to have $d_\sigma^2<16$.

The lateral and longitudinal profiles of each shower were required to be consistent with those expected for a single isolated electron incident along the track direction as determined from test beam data. From the observed and expected quantities and their estimated errors, a χ^2 test for the electron hypothesis was defined. Since most of the experimental distributions have non-gaussian tails, $P(\chi^2)$ is not a true χ^2 probability but can be considered as a quality factor. Electron candidates with $P(\chi^2)<10^{-4}$ were rejected. The efficiencies for these selection criteria are described in detail in ref. [10].

The electron energy was corrected for the impact point and track direction dependence of the calorimeter response and for the average energy loss in the preshower detectors. These corrections use the energy deposited in those cells which are expected to contain a large fraction of the total electron energy

(typically two cells), and apply an additional correction for the energy expected outside this "core" region. This algorithm minimizes the influence of particles produced in association with the W or Z (underlying event) on the reconstructed electron energy without degrading the electron resolution. An average transverse energy shift of $+120\pm20$ MeV due to the presence of underlying event energy in the core region has been measured for electrons from $W\to e\nu$ decays.

3.2. Neutrino measurement

The determination of the neutrino momentum in $W\to e\nu$ decays is made indirectly by measuring the energy of the particles which recoil against the W. The missing momentum is attributed to the undetected neutrino:

$$\boldsymbol{P}(\nu)\simeq-[\boldsymbol{P}(e)+\boldsymbol{P}(\text{hadrons})]\,.$$

A measurement of the longitudinal component (P_L) for the neutrino would require the accurate measurement of P_L for all of the hadrons in the event. These hadrons arise both from fragmentation of the spectator partons, and from initial state bremsstrahlung from the hard scattering process. Both classes of hadrons carry significant amounts of longitudinal momentum, whereas the spectators carry very little transverse momentum. The hadrons produced by spectator partons are often too close to the incoming beam directions to be measurable, precluding any useful reconstruction of $P_L(\nu)$, but leaving the $P_T(\nu)$ reconstruction largely unaffected.

The neutrino transverse momentum was estimated from the transverse component of the momentum balance:

$$\boldsymbol{P}_T(\nu)\equiv-[\boldsymbol{P}_T(e)+\boldsymbol{P}_T(\text{hadrons})]$$

$$=-\boldsymbol{P}_T(e)-\left[\sum E(\text{cell})\cdot\boldsymbol{v}(\text{cell})\right]_T,$$

where $\boldsymbol{v}$(cell) is a unit vector from the interaction vertex to the cell center, E(cell) is the weighted sum of compartment energies for the cell, and $\boldsymbol{P}_T(e)$ is the electron transverse momentum corrected for the impact point. To avoid double-counting, the sum over cells includes only those cells outside the electron core region, and the electron energy includes the corrected energy for those cells inside the core region. There is a small amount of energy from the electron which leaks out of this core (typically 1%), and a small amount of underlying event energy which flows into the core. These two effects are the major sources of systematic difference between the energy scale of the neutrino and that of the electron. Using the definition above, the W transverse momentum is approximated by $\boldsymbol{P}_T(W)\simeq-\boldsymbol{P}_T(\text{hadrons})$.

4. The data samples

The electron selection described in section 3.1 was used to provide an initial sample of events. Because of the high quality of energy reconstruction demanded for this analysis, some further fiducial cuts have also been applied:

- W and Z candidates in which one or both of the electrons hit an edge cell ($0.8\leqslant|\eta|\leqslant1.0$) of the central calorimeter have been removed. These cells have significantly poorer energy resolution due to the modifications required for the new central tracking detectors [8].
- W and Z candidates in which one or both of the electrons hit close to a cell boundary have been removed. In the central calorimeter, this region of the cell requires the largest energy corrections and suffers from non-gaussian energy resolution. The cut eliminates 15% of the total surface area of a central calorimeter cell.
- W candidates with $P_T(W)$ larger than 20 GeV have been removed. Their neutrino measurement error is larger owing to the large hadronic energy produced in association with the W. This requirement eliminates roughly 5% of the sample.

4.1. The W sample

A kinematic selection was used to ensure that the W sample contained negligible QCD background (estimated to be $<1\%$ in ref. [10]):

$$20<P_T(e)<60\ \text{GeV}\,,$$

$$20<P_T(\nu)<60\ \text{GeV}\,,$$

$$40<m_T<120\ \text{GeV}\,,$$

where the transverse mass, m_T, was defined to be

$m_T^2 = 2P_T(e)P_T(\nu)(1-\cos\phi_{e\nu})$,

and $\phi_{e\nu}$ is the angle between $\boldsymbol{P}_T(e)$ and $\boldsymbol{P}_T(\nu)$. These selection criteria resulted in a W sample of 1203 events with the electron in the central calorimeter, shown in fig. 1 and fig. 2, and 344 events with a forward electron. These samples arise predominantly from the process $W\to e\nu$. However, the central and forward samples are expected to contain an additional contribution of 3.8% and 3.3% respectively, from the process $W\to\tau\nu$ followed by the decay $\tau\to e\nu\bar{\nu}$.

4.2. The Z sample

Events in the Z sample were required to lie in the range

$70 < m_{ee} < 120$ GeV ,

where m_{ee} was defined to be the invariant mass of the electron pair. At most one of the central electron tracks was allowed to satisfy the looser tracking criteria defined in ref. [10], leading to a sample with an estimated background of $<1\%$. If the event contained a third electromagnetic cluster with $E_T > 5$ GeV, a three body mass was computed to improve the accuracy of the measurement for $Z\to\gamma e^+e^-$ events. The Z selection resulted in 54 events with both electrons in the central calorimeter, shown in fig. 3a,

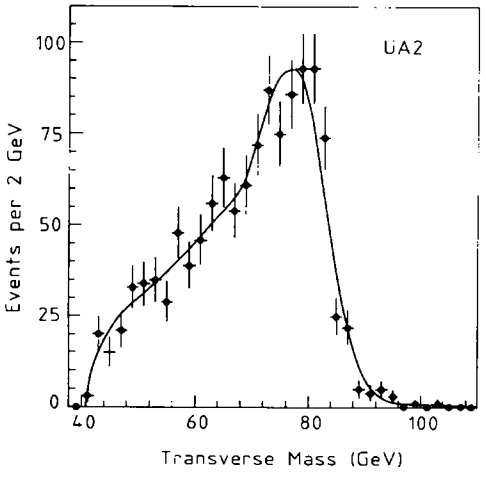

Fig. 1. The fit to the transverse mass distribution for the W sample with the fitted curve superimposed.

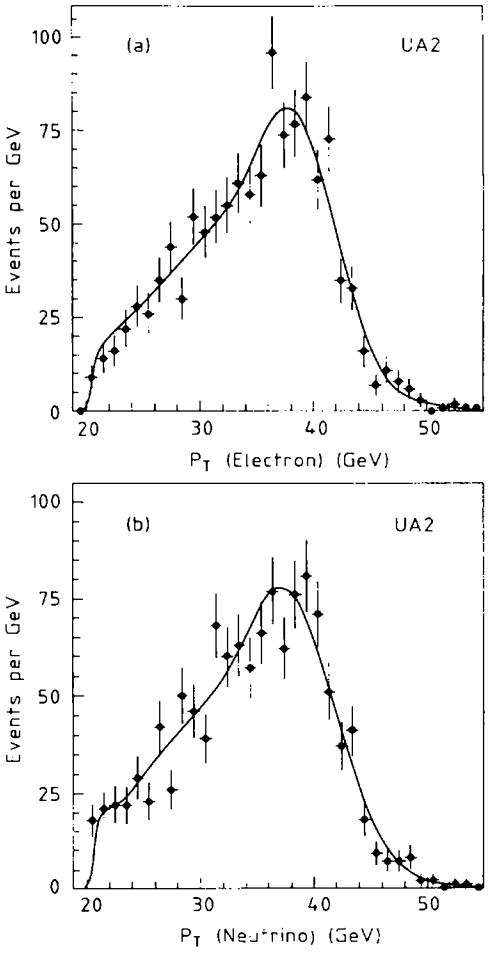

Fig. 2. The fits to the transverse momentum distributions for the W sample with the fitted curves superimposed. (a) The $P_T(e)$ distribution, (b) the $P_T(\nu)$ distribution.

of which one contained an extra photon. There were 40 events with one electron in the endcap calorimeters, and 8 events with both electrons in the endcap calorimeters.

Ideally, all of these samples would be included in the measurement of the boson masses. However, the ultimate goal is to measure the ratio of the masses with the smallest possible errors, and due to the different energy reconstruction uncertainties in the endcap and central calorimeters [8], the systematic errors are not identical. In addition, the different relative populations of W and Z events in these calorimeters imply that, if the systematic errors are dif-

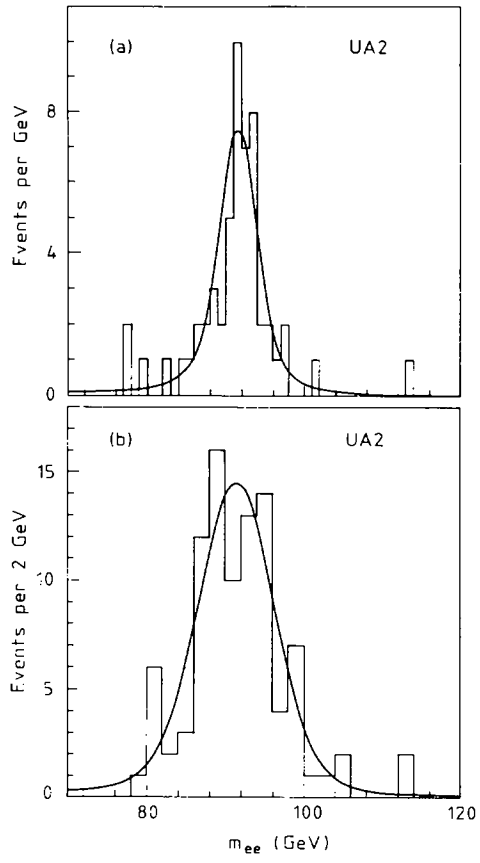

Fig. 3. The fit to the invariant mass distributions for the Z samples with the fitted curves superimposed. (a) The central Z sample, (b) the P_T(constrained) Z sample.

ferent, they will not cancel in taking the mass ratio. For these reasons, the present analysis uses only those W and Z events in which the electron energy is measured in the central calorimeter fiducial volume.

In order to reduce the statistical error on the m_Z measurement, an additional sample of Z events has been defined in which one electron was required to be in the central fiducial region, and the second one had to be outside this region (thereby including those electrons which hit the central calorimeter but fail the fiducial cuts defined previously, in addition to those which hit the endcap calorimeters). These events have the energy of their second electron constrained by the requirement that the total momentum (electrons plus hadrons) is balanced along a particular direction in the transverse plane. For this purpose, a coordinate system was defined with axes parallel to the bisector of the two electron transverse directions (η axis), and orthogonal to it (ξ axis). For a Z event with relatively low P_T, the momentum balance along the ξ axis is sensitive to the electron energies, and the ξ direction is not strongly correlated with that of the recoiling hadrons, thus providing a useful constraint. The result of this constraint procedure, including the mass requirement defined above, is an independent sample of 94 Z events which have worse mass resolution, but which derive their mass scale from the energy calibration of the central calorimeter fiducial volume. This sample is shown in fig. 3b and will be referred to as the P_T(constrained) sample.

5. The fitting procedure

The masses of the W and Z have been measured using a maximum likelihood fitting procedure.

For the $Z \rightarrow e^+e^-$ decay, the two leptons were unambiguously measured, and therefore the extraction of the Z mass from the observed distribution of m_{ee} was relatively simple. It was possible to use an analytic likelihood function which is a good approximation to the expected line shape, followed by small corrections for the effects which were neglected in the simplified function.

For the $W \rightarrow e\nu$ decay, the neutrino was measured indirectly, using the method described in section 3.2. Since the longitudinal momentum of the neutrino cannot be measured, the variables which have been considered in this analysis are the transverse momenta $P_T(e)$ and $P_T(\nu)$, and the transverse mass, m_T. For these variables, the shape of the distribution expected for a given value of the W mass depends critically on the detector resolution and on the P_T distribution of the produced W boson. To a lesser extent, the shape also depends on the P_L distribution for the W, and hence on the parton distribution functions for the incoming hadrons. These considerations do not allow the use of analytic functions in fitting the W mass. Instead, the likelihood functions for different measured quantities were constructed numerically using a detailed simulation of W production and decay, followed by a carefully tuned model of the detector response to the W decay products, implemented in the form of a Monte Carlo simulation which was

optimized for the fitting problem. This Monte Carlo was designed to efficiently generate large statistical samples to provide stable likelihood functions. It was also highly tunable in order to evaluate the effects of systematic uncertainties associated with the many ingredients of the model.

5.1. Physics and detector model

The Monte Carlo can generate all of the basic processes which are relevant to this analysis. For the W, the basic processes are $W\to e\nu$ and $W\to\tau\nu$. However, due to the high precision of the current study, it was necessary to consider QED corrections. Such corrections [11] produce $W\to\gamma e\nu$ decays, where a low energy photon may carry off some of the electron energy and thereby change the reconstructed mass. For the Z, the basic process is $Z\to e^+e^-$, and QED corrections result in the decay $Z\to\gamma e^+e^-$. All of these processes can be generated starting from one of many sets of parton distribution functions evolved to $Q^2=m_W^2$ or m_Z^2. The DFLM set [12] with $\Lambda_{QCD}=160$ MeV has been used to obtain the final results, but other sets have been studied for the evaluation of systematic errors presented in section 6.

The W or Z boson was produced with a transverse momentum distribution derived from the calculations performed in ref. [13]. In order to vary the shape of the P_T distribution, different calculations have been performed, corresponding to different values for Λ_{QCD} of 110, 160, 210, and 260 MeV. In these calculations, the value for the strong coupling constant has been computed using Λ_{QCD}, and the DFLM parametrization which had the closest corresponding Λ_{QCD} value was chosen. Changing the value of Λ_{QCD} primarily alters the scale of the distribution; larger values correspond to a harder distribution for the P_T of the boson [14]. In choosing this approach it has been assumed that the underlying calculation in ref. [13] gives a good description of the data, and that uncertainties in the true P_T distribution can be contained in the band of variations obtained by varying Λ_{QCD}.

Once the kinematics of a given event were fixed, the calorimeter impact points for the electrons were calculated using the observed vertex distribution, and the requirement that the electrons pass through the fiducial regions of the tracking systems was imposed.

The detector response was simulated by first applying a detailed model for the electron response, derived from test beam data, to compute the observed electron energy. This was followed by the difficult step of simulating the neutrino response. As discussed in section 3.2, the neutrino response consists of a component coming from the electron response, and a component coming from the use of P_T(hadrons) to approximate P_T(boson). The measurement process for P_T(hadrons) is described in more detail in ref. [14], and a summary of the salient results is provided here.

The model which has been constructed contains two basic ingredients. The first is a resolution function which reflects the cumulative effect of the individual calorimeter measurements that are summed to give P_T(hadrons). This resolution depends on the total transverse energy in the event ($\sum E_T$), excluding the boson decay products. Studies of different data samples have been used to derive the resolution function, together with an estimate of its uncertainties. The second ingredient is a response correction function which reflects the systematic mismeasurement made in approximating P_T(boson) by P_T(hadrons). This arises primarily from the detector acceptance (some recoiling hadrons, especially those associated with initial state bremsstrahlung, flow outside the calorimeter acceptance), and from calorimeter nonlinearities which appear when P_T(hadrons) is constructed from a sum of calorimeter cell measurements. A functional form for these effects has been derived from Monte Carlo studies.

The ingredients of the model have been checked by studying the momentum balance between the electrons and the recoiling hadrons in $Z\to e^+e^-$ events. In particular, if this balance is measured along the η axis defined in section 4.2, then the effects of the electron energy resolution are largely removed (the resolution for $P_T^{\eta}(e^+e^-)$ is ~ 0.3 GeV, while for $P_T^{\xi}(e^+e^-)$ it is ~ 2 GeV). A special data sample was defined, corresponding to the kinematic region relevant for this analysis, namely $70\leqslant m_{ee}\leqslant 120$ GeV and $P_T(Z)\leqslant 20$ GeV. Since this choice of the measurement axis minimizes the sensitivity to the electron energy measurement, it was possible to remove the fiducial cuts on the cell boundaries, resulting in a larger sample of 161 events. Events of the type $Z\to\gamma e^+e^-$ have been excluded from this sample be-

cause the electrons do not carry the full Z momentum. The momentum balance is shown in fig. 4a. In this figure, the resolution function should account for the width of the observed distribution whereas the response function should account for the displacement of the mean. The resolution was checked by looking at a normalized distribution where for each event the observed momentum balance is divided by the expected resolution computed using the $\sum E_T$ for that event. The resulting distribution should have a sigma of 1.0 if the resolution function is correct. The observed sigma is 0.98 ± 0.11, in excellent agreement with expectations. In order to probe the momentum balance for information about the response correction, the influence of statistical fluctuations has been minimized by examining the cumulative distribution. This is shown in fig. 4b, where additional curves have been superimposed to show the extreme variations. The construction of the allowed band of variations for each of the model ingredients above is crucial in constraining possible variations in the neutrino response, and forms the basis of the systematic error analysis presented in section 6.

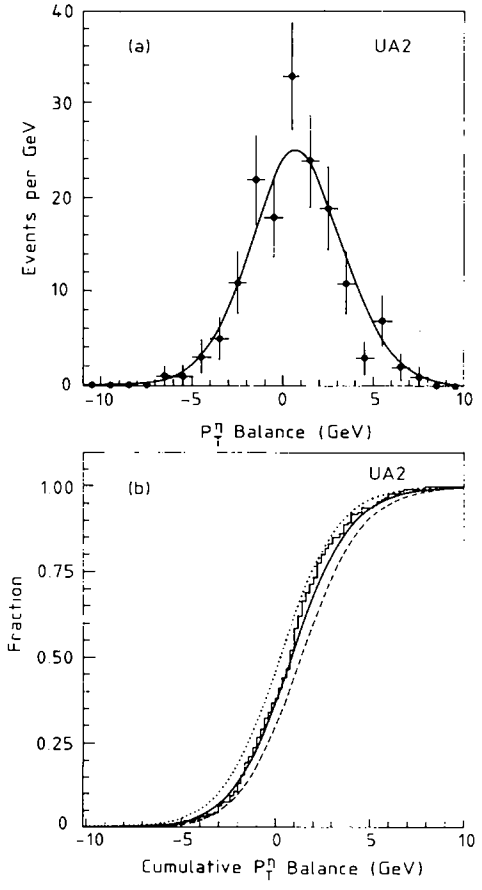

Fig. 4. The momentum balance observed in $Z \rightarrow e^+e^-$ events along the η axis. (a) The distribution for the data where the curve corresponds to the prediction of the model described in the text. (b) The cumulative distribution where the dotted (dashed) curves represent the minimal (maximal) response corrections.

Finally, the dependence on the mass and width of the produced boson was introduced. In order to construct the continuous functions needed for fitting in an efficient manner, the same event was weighted by a relativistic Breit–Wigner line shape for many different values of the mass and width, and then simultaneously entered into a two dimensional array of distributions corresponding to these different mass and width values.

5.2. Procedure for the m_W fit

The fitting procedure started from the two dimensional array of distributions generated by the model for a given fitting variable, for example, m_T. These distributions were smoothed and interpolated to provide a continuous function $f(m_T; m_W, \Gamma_W)$, which represents the likelihood to observe the given value of m_T for particular values of the fitting parameters m_W and Γ_W. Such a function was used to compute a global likelihood defined as the product of the likelihood values for each event in the fit sample. It should be noted that although this method treats each event separately, without binning, it assumes that all events in the sample have the average resolution.

Since the maximum likelihood method provides no explicit information about the quality of the fit, it is necessary to adopt an additional method to test for the goodness-of-fit. The Kolmogorov–Smirnov test has been selected, based on the maximum distance between the cumulative distribution of the data and that of the best fit result. This test is known to be suitable for small samples, and does not impose any binning requirement on the data.

5.3. Procedure for the m_Z fit

For the case of the Z, the numerical likelihood technique described above for the W could easily be applied. However, due to the relative simplicity of this fit, an approximate analytic method has been used, based on the analytic function

$$f(m_{ee}, \sigma, m_Z, \Gamma_Z) \simeq \int dm' \frac{\exp(-\beta m')}{(m'-m_Z)^2+\Gamma_Z^2/4} \times \exp[-(m_{ee}-m')^2/2\sigma^2] ,$$

where σ is the estimated mass resolution for the event considered, and β is a slope parameter which was obtained by fitting Monte Carlo spectra. This function contains a non-relativistic Breit–Wigner line shape, distorted by the rapidly falling parton luminosity characteristic of hadron colliders. The true shape is more accurately described by a relativistic Breit–Wigner including an energy dependent width [15]; the form used in this analysis results in a shift of the peak by +17 MeV relative to the more complete form. The exponential approximation for the parton luminosity has been adopted because it allows the convolution integral to be performed analytically and provides an excellent representation of the actual shape. The slope parameter used was $\beta = 0.0200 \pm 0.0005$, where the error reflects the variation observed when fitting different parton distribution parametrizations. If the parameter β was neglected for the mass interval used in this analysis, the resulting fit mass was observed to shift by $\simeq -120$ MeV. The effects of the experimental resolution are included by convoluting the underlying line shape with a gaussian. With the use of this explicit resolution function, it becomes possible to weight the contribution of each event according to its measurement error, and hence to make optimal use of the small Z event sample.

6. Results

6.1. Measurement of m_Z

Before applying the fitting procedure defined in section 5 to the two data samples defined in section 4.2, an estimate of the measurement error for the mass of each event is required. For the central sample, this error depends on the electron measurement alone. Special test beam runs were performed, where the test beam direction was defined by the observed direction and impact point for each electron in 46 of the 54 events in the central sample. These measurements provide values for the measurement errors which agree very well with those predicted by the model defined in section 5.1, and constitute an important check of the energy correction procedure for this event sample. The model was used to compute the errors for the remaining 8 events. A mean measurement error of 1.9 GeV with a RMS of 0.2 GeV resulted for the full sample. For the P_T(constrained) sample, the errors arise largely from the measurement of the recoiling hadrons, and have been computed directly from the model, resulting in a rather broad distribution with a mean of 4.3 GeV and a RMS of 0.8 GeV.

These samples and their errors have been studied using two different fits. In the first, the width of the Z is fixed to 2.5 GeV, as expected in the standard model when $Z \to t\bar{t}$ decays are kinematically forbidden. This fit is shown for the central sample in fig. 3a, and for the P_T(constrained) sample in fig. 3b. For the second fit, the width is left free, providing a test of assumptions in the first fit. The results are summarized in table 1. They must be corrected for effects which have been neglected in the fit, and all of the

Table 1
A summary of the fits to different Z samples. The error shown is the statistical error from the fit.

Sample	1 Parameter fit			2 Parameter fit		
	m_Z (GeV)	Γ_Z (GeV)	Confidence level (%)	m_Z (GeV)	Γ_Z (GeV)	Confidence level (%)
central (analytic method)	91.69 ± 0.43	2.5	96	91.70 ± 0.45	$2.96^{+0.98}_{-0.78}$	99
P_T(constrained) (analytic method)	91.51 ± 0.57	2.5	96	91.53 ± 0.59	$2.94^{+1.18}_{-0.94}$	97
central (numeric method)	91.71 ± 0.48	2.5	95	91.72 ± 0.50	$3.06^{+0.98}_{-0.87}$	84

systematic uncertainties must be tabulated. These corrections have been evaluated for the central sample, and have been checked for the P_T(constrained) sample, allowing the use of a common set of corrections for the two fits. The effects considered were:

(1) The effect of the underlying event on the electron energy scale has been studied using two large correlated samples of Monte Carlo events, one including the effect and one ignoring it. These samples were divided into realistic sub-samples which were fitted using the same method used for the data. The difference between fits to the two samples serves as a measure of the effect, leading to the correction

$$\Delta m = -240 \pm 70 \text{ MeV},$$

where the error quoted includes the effect of the small data samples.

(2) The effect of radiative decays on the fitted mass has been estimated by a Monte Carlo simulation of the $Z \to \gamma e^+ e^-$ process [11] which includes the response of the detector to the low energy photon. This response has not been measured directly, but is extrapolated from that measured for test beam electrons. The resulting shift in the fitted mass is

$$\Delta m = +100 \pm 100 \text{ MeV},$$

where the large systematic error has been assigned to account for the uncertainties in the detector response to low energy photons.

(3) For the P_T(constrained) sample, the observed mass depends on the measurement of P_T(hadrons). The effect of the measurement model for P_T(hadrons) has been studied by varying the resolution and response corrections within the limits described in section 5.1. Large samples of Monte Carlo events were generated and fitted, and the observed variations in the fitted mass were confined to ± 100 MeV from the nominal value.

These effects lead to an overall correction of -140 MeV and an overall systematic error of 120 MeV. The additional systematic error of 100 MeV for the P_T(constrained) fit has been added in quadrature with the corresponding statistical error. The final Z mass is computed by taking a weighted average of the two one parameter analytic fits in table 1. The result is

$$m_Z = 91.49 \pm 0.35(\text{stat}) \pm 0.12(\text{syst}) \pm 0.92(\text{scale}) \text{ GeV},$$

where a scale error of 1.0% has been included, reflecting the systematic uncertainty in the energy calibration of the central calorimeter fiducial volume [8].

Several tests have been performed to confirm the result reported above. The first involved generating large Monte Carlo samples with given m_Z and Γ_Z, and studying the behavior of the fitting procedure. This was done with a single large sample to check that there were no systematic biases in the procedure, and then with many sub-samples of 54 or 94 events to confirm that the procedure does, on average, reconstruct the correct mass, and that the distribution of fitted masses is consistent with the errors predicted by the likelihood fit. As a by-product of this study, distributions of the expected likelihood and confidence level for these ideal samples were compared with the fits to the data, confirming that the observed results agree with expectations. In addition, the data samples were fitted using the numerical likelihood method developed for the W case. The results of these fits, for the central sample only, are shown in table 1. They are very consistent with those found using the analytic likelihood method. Additional fits have been performed using a large Monte Carlo control sample to measure the effect of including items (1) and (2) in the numeric likelihood method. The results were -230 MeV for item (1), and $+80$ MeV for item (2), in excellent agreement with the previous estimates. Further checks have been made by including the effect of interference between the Z and the Drell–Yan continuum in the likelihood function, resulting in a negligible shift of $+25$ MeV in the fitted mass. As a final check, the mass interval defined in section 4.2 was changed to $80 < m_{ee} < 110$ GeV with a resulting change in the combined mass of -40 MeV.

6.2. Measurement of m_W

The central W sample defined in section 4.1 has been studied using two different fits to the three kinematic variables. In the first, the width of the W is fixed to 2.1 GeV, as expected in the standard model when $W \to t\bar{b}$ decays are kinematically forbidden. This fit is shown for the transverse mass distribution in fig. 1, and for the two transverse momentum distributions in fig. 2. For the second fit, the width has been left free. The results of these fits are summarized in table 2.

Table 2
A summary of the fits to different W distributions. The error shown is the statistical error from the fit.

Sample	1 Parameter fit			2 Parameter fit		
	m_W (GeV)	Γ_W (GeV)	Confidence level (%)	m_W (GeV)	Γ_W (GeV)	Confidence level (%)
transverse mass	80.75 ± 0.31	2.1	84	80.78 ± 0.31	$1.89^{+0.47}_{0.40}$	89
P_T (electron)	80.79 ± 0.38	2.1	95	80.83 ± 0.39	$1.60^{+0.78}_{-0.68}$	97
P_T (neutrino)	80.32 ± 0.41	2.1	83	80.33 ± 0.42	$2.03^{+0.82}_{-0.72}$	88

The analysis of the systematic uncertainties affecting the W mass measurement is complex. It is rendered especially difficult by the need to reliably evaluate systematic effects which are small compared to the statistical errors of the fits. Trying to measure these shifts by changing the event selection cuts leads to results which are confused by statistical fluctuations. To avoid these difficulties, the approach used has been to change some of the model parameters and generate new likelihood functions for each such variation. These different functions were probed by fitting two constant data samples. The first was the observed data sample of 1203 events, and the second was a 5000 event sample of Monte Carlo data generated using the default model parameters. Using this technique, it appears possible to evaluate systematic errors with a precision of at least 50 MeV.

The corrections and uncertainties considered in the W mass measurement are summarized in table 3, where the observed shifts in the fitted m_W value for one parameter fits to the Monte Carlo control sample are tabulated. A brief discussion of the sources for these variations is given below:

(1) The largest uncertainties are associated with the lack of knowledge of the true $P_T(W)$ distribution, and the detector response to the recoiling hadrons. With a tenfold increase in the available sample of $Z \to e^+e^-$ events, these unknowns could be tightly constrained using the momentum balance shown in fig. 4 and the observed $P_T(Z)$ distribution; with the present statistics, the uncertainties remain significant. In order to quantify this, allowed regions for the theoretical and experimental uncertainties have been defined. The extreme parametrizations of the resolution and response functions discussed in section 5.1 define the experimental uncertainties. A range for Λ_{QCD} has been defined using the observed $P_T(W)$ and $P_T(Z)$ distributions [14] to quantify the theoretical uncertainty. Variations outside the range $110 \leqslant \Lambda_{QCD} \leqslant 210$ MeV lead to significant disagreements with one of these distributions. A series of eight variations have been performed, spanning the allowed ranges. The maximum positive and negative deviations have been averaged to give the values in table 3. For this set of variations, the average $P_T(\nu)$ resolution varies within the range $3.0^{+0.4}_{-0.3}$ GeV and the

Table 3
A summary of the corrections and systematic errors for each of the W mass fits. All values are in MeV.

Model variation	m_T fit	$P_T(e)$ fit	$P_T(\nu)$ fit
(1) hadron resolution/response and P_T(boson) distribution	± 115	± 215	± 350
(2) parton distributions	$+100$	± 160	± 130
(3) neutrino scale	± 85	–	± 170
(4) electron resolution	± 40	± 50	± 60
(5) underlying event	± 30	± 50	± 20
(6) fit procedure	± 100	$+100$	± 150
(7) radiative decays	$+40 \pm 40$	$+60 \pm 60$	$+160 \pm 160$
total	$+40 \pm 210$	$+60 \pm 300$	$+160 \pm 470$

average m_T resolution varies in the range 3.5 ± 0.2 GeV. It should also be noted that fits to the data performed using some of these variations resulted in values for Γ_W from the three different fits which were inconsistent with each other, lending further support to the consideration of these variations as extremes.

(2) The effects of parton distribution function uncertainties have been studied using the recent DFLM, MRSE′ and MRSB′ sets [16], and the older EHLQ [17] and Duke–Owens [18] sets. The maximum variations observed have been retained. However, this may overestimate the actual uncertainty since the older sets agree poorly with current data on the ratio of u and d valence quarks in the proton [19]. Excluding the EHLQ and Duke–Owens sets reduces the observed variations by only 25%.

(3) The uncertainties in the energy scale for the neutrino which are inherited from the electron measurement will cancel when computing the mass ratio. In addition, the hadron energy scale has a negligible effect on the neutrino scale, because the neutrino direction is not correlated with the direction of the recoiling hadrons. However, additional effects, discussed in section 3.2, lead to the estimates given in table 3.

(4) The uncertainty on the electron energy resolution, as determined from test beam data, was estimated to be less than 10%. The average $P_T(e)$ resolution was 1.2 GeV, so such variations have a small effect.

(5) Variations in the underlying event contribution to the electron energy scale, described in section 3.1, are observed to have a small effect.

(6) Variations in the procedures used to construct the numerical likelihood functions lead to changes in the fitted results due to the finite Monte Carlo statistics available. Such variations have been studied by fitting a control sample of 15 000 Monte Carlo events to check for systematic biases, and could be reduced by using significantly larger Monte Carlo samples to construct the likelihood functions.

(7) The effects of radiative decays $W \to \gamma e \nu$ have been considered. The large systematic errors assigned reflect the poorly known detector response to low energy photons.

The variations listed in table 3 have been treated as gaussian systematic errors, and added in quadrature to calculate the total systematic error. The corrections listed in table 3 have added to the one parameter fit results in table 2, leading to the final results for the W mass fits:

$$m_W = 80.79 \pm 0.31\,(\text{stat}) \pm 0.21\,(\text{syst})\ \text{GeV}$$
$$(m_T\ \text{fit}),$$
$$m_W = 80.85 \pm 0.38\,(\text{stat}) \pm 0.30\,(\text{syst})\ \text{GeV}$$
$$(P_T(e)\ \text{fit}),$$
$$m_W = 80.48 \pm 0.41\,(\text{stat}) \pm 0.47\,(\text{syst})\ \text{GeV}$$
$$(P_T(\nu)\ \text{fit}).$$

The fit to the transverse mass is observed to have smallest statistical and systematic errors, and has been taken as the final value. The other two fits provide a significant cross-check of the method. The statistical errors for the fits are strongly correlated, but the results are quite consistent within the systematic errors alone. The final value for the W mass is then given by

$$m_W = 80.79 \pm 0.31\,(\text{stat}) \pm 0.21\,(\text{syst}) \pm 0.81\,(\text{scale})\ \text{GeV},$$

where the 1% scale error has been included.

6.3. Measurement of m_W/m_Z

The two measurements of the boson masses can be combined to derive a value for m_W/m_Z. One expects an almost perfect cancellation of the energy scale contribution to the error on the ratio. Deviations from this expectation can arise if the calorimeter response to electrons is not perfectly linear, since the electrons produced in Z decays are, on average, more energetic than those found in W decays. Possible non-linearities in the UA2 calorimetry have been minimized by choosing an energy of 40 GeV, which is close to the mean value expected for W and Z decays, as the test beam energy that establishes the absolute calibration. Any residual effect is estimated to contribute less than 100 MeV to the mass difference, and is therefore ignored in computing the ratio.

Thus the mass ratio becomes

$$m_W/m_Z = 0.8831 \pm 0.0048\,(\text{stat}) \pm 0.0026\,(\text{syst}).$$

This can be combined with the most recent results

from LEP and SLC [2] for the Z mass (a weighted average of $m_Z = 91.150 \pm 0.032$ GeV, including the current 30 MeV uncertainty in the LEP energy scale, was used) to give a rescaled W mass:

$$m_W = 80.49 \pm 0.43(\text{stat}) \pm 0.24(\text{syst}) \text{ GeV},$$

which can be compared with the value expected from the standard model.

7. Comparison with the standard model

In the standard model of the electroweak interactions, with a minimal Higgs sector, there are three fundamental free parameters (ignoring the Higgs and fermion masses). A convenient choice for these parameters, which reflects the precision of current measurements, is

$$\alpha, \quad G_\mu, \quad m_Z .$$

A renormalization scheme must be chosen for the computation of higher order corrections. In this analysis, the scheme of Sirlin [20] is used:

$$\sin^2\theta_w \equiv 1 - \frac{m_W^2}{m_Z^2},$$

leading to standard relations [21] among the fundamental parameters:

$$m_W^2 = \frac{A^2}{(1-\Delta r)\sin^2\theta_w},$$

$$m_Z^2 = \frac{A^2}{(1-\Delta r)\sin^2\theta_w \cos^2\theta_w},$$

where

$$A \equiv \left(\frac{\pi\alpha}{\sqrt{2}\, G_\mu}\right)^{1/2} = 37.2805 \pm 0.0003 \text{ GeV}$$

can be computed from current measurements of α and G_μ [22]. The variable Δr represents the radiative corrections arising from virtual loops in the boson propagators, and depends on the unknown masses m_{top} and m_{Higgs}. These corrections have been calculated within the context of the minimal standard model, containing a single complex Higgs doublet, and an accurate numerical value can be computed using the program of Hollik and Burgers [23].

Using the relations defined above, it is possible, given values for the Z mass and Δr, to predict a value for the W mass. This can be seen in fig. 5, where the dependence of Δr on m_{top} and m_{Higgs} is indicated by a series of lines in the (m_W, m_Z) plane. The strong dependence on m_{top} arises because the top quark is a member of a doublet with a large mass splitting [24]. The UA2 result, in combination with that of LEP and SLC, has been marked by a data point whose errors reflect the combined statistical and systematic errors on the measurements. This data point lies within the region of the plane allowed by the minimal standard model, and gives further support to a top quark which is heavier than the W. To quantify this statement, a value for Δr has been computed from the m_W/m_Z measurement combined with the LEP and SLC value for m_Z. The result is

$$\Delta r = 0.026^{+0.029}_{-0.032},$$

where the asymmetric error includes the statistical and systematic errors for the two input measurements. Symmetric confidence intervals have been determined:

$$-0.016(-0.029) < \Delta r < 0.062(0.071)$$

at 80(90)% confidence level.

Within the context of the minimal standard model,

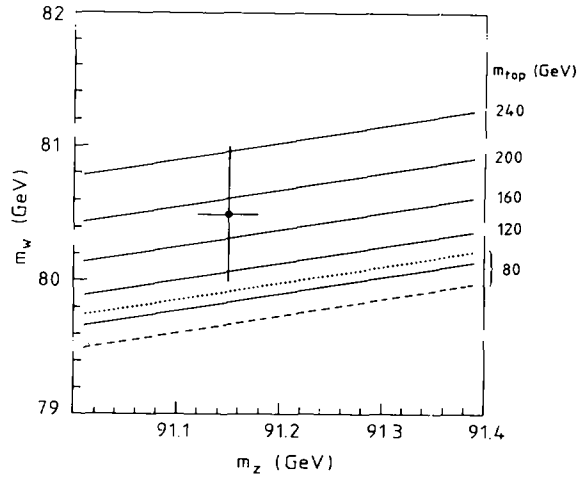

Fig. 5. The comparison with the minimal standard model predictions. The solid lines indicate the allowed values for m_W and m_Z for a given m_{top} with $m_{Higgs} = 100$ GeV. The dotted (dashed) line indicates the prediction for $m_{top} = 80$ GeV with $m_{Higgs} = 10$ (1000) GeV. The data point is defined in the text.

these intervals can be used to provide limits on m_{top}, assuming $m_Z = 91.150$ GeV, and taking a conservative allowed region for m_{Higgs}. Recent LEP results [25] indicate that $m_{Higgs} > 24$ GeV. Using this constraint leads to the lower limit

$m_{top} > 76$ GeV at 90% confidence level

for $m_{Higgs} \geq 24$ GeV .

No limit exists at the 95% confidence level for the stated range of m_{Higgs}. A corresponding upper limit can be derived:

$m_{top} < 272(289)$ GeV at 90(95)% confidence level

for $m_{Higgs} \leq 1000$ GeV .

However, it should be noted that the presence of additional fermion doublets or Higgs multiplets, beyond those present in the minimal standard model, can substantially modify the value of Δr, reducing the predictive power of fig. 5, and eliminating any limit on m_{top}.

Finally, the definition for the weak mixing angle given above can be used to convert the measurement of m_W/m_Z to a measurement of $\sin^2\theta_w$:

$$\sin^2\theta_w = 0.2202 \pm 0.0084(\text{stat}) \pm 0.0045(\text{syst}) ,$$

which is consistent with the world average value [26] derived from neutral current experiments:

$$\sin^2\theta_w = 0.2309 \pm 0.0029(\text{stat}) \pm 0.0049(\text{syst}) .$$

8. Conclusions

Precise values for the W and Z masses have been measured from large samples of $W \to e\nu$ and $Z \to e^+e^-$ events accumulated by the upgraded UA2 detector. After a careful analysis of systematic errors, an improved result is obtained for the mass ratio $m_W/m_Z = 0.8831 \pm 0.0048(\text{stat}) \pm 0.0026(\text{syst})$. This has been combined with recent measurements of the Z mass from LEP and SLC to give an absolute measurement of the W mass $m_W = 80.49 \pm 0.43(\text{stat}) \pm 0.24(\text{syst})$ GeV. A new value for the weak mixing parameter, $\sin^2\theta_w = 0.2202 \pm 0.0084(\text{stat}) \pm 0.0045(\text{syst})$, has also been reported. The results of these measurements are in good agreement with the minimal standard model, and give further support to the hypothesis that the top quark is heavier than the W.

Acknowledgement

We gratefully acknowledge P. Darriulat for his contributions and guidance during the design and construction of the UA2 upgrade project. The technical staff of the institutes collaborating in UA2 have contributed substantially to the construction and operation of the experiment. We deeply thank them for their continuous support. The experiment would not have been possible without the very successful operation of the improved CERN $\bar{p}p$ Collider whose staff and coordinators we sincerely thank for their collective effort. Financial support from the Schweizerischen Nationalfonds zur Förderung der Wissenschaftlichen Forschung to the Bern group, from the UK Science and Engineering Research Council to the Cambridge group, from the Bundesministerium für Forschung und Technologie to the Heidelberg group, from the Institut National de Physique Nucléaire et de Physique des Particles to the Orsay group, from the Istituto Nazionale di Fisica Nucleare to the Milano, Pavia, Perugia and Pisa groups and from the Institut de Recherche Fondamentale (CEA) to the Saclay group are acknowledged.

References

[1] UA1 Collab., G. Arnison et al., Phys. Lett. B 122 (1983) 103; Phys. Lett. B 126 (1983) 398;
UA2 Collab., M. Banner et al., Phys. Lett. B 122 (1983) 476;
UA2 Collab., P. Bagnaia et al., Phys. Lett. B 129 (1983) 130.

[2] Mark II Collab., G. Abrams et al., Phys. Rev. Lett. 63 (1989) 2173;
ALEPH Collab., D. Decamp et al., Phys. Lett. B 231 (1989) 519; B 235 (1990) 399;
DELPHI Collab., P. Aarnio et al., Phys. Lett. B 231 (1989) 539;
L3 Collab., B. Adeva et al., Phys. Lett. B 231 (1989) 509; B 237 (1990) 136;
OPAL Collab., M.Z. Akrawy et al., Phys. Lett. B 231 (1989) 530.

[3] R. Ansari et al., Nucl. Instrum. Methods A 279 (1989) 388.

[4] F. Bosi et al., Nucl. Instrum. Methods A 283 (1989) 532.

[5] R. Ansorge et al., Nucl. Instrum. Methods A 265 (1988) 33;
J. Alitti et al., Nucl. Instrum. Methods A 279 (1989) 364.
[6] K. Borer et al., Nucl. Instrum. Methods A 286 (1990) 128.
[7] A. Beer et al., Nucl. Instrum. Methods A 224 (1984) 360.
[8] F. Alberio et al., The electron, jet, and missing transverse energy calorimetry of the upgraded UA2 experiment at the CERN $\bar{p}p$ collider, in preparation for Nucl. Instrum. Methods.
[9] G. Blaylock et al., The multi-level trigger and data acquisition system of the upgraded UA2 experiment at the CERN $\bar{p}p$ collider, in preparation for Nucl. Instrum. Methods.
[10] UA2 Collab., J. Alitti et al., Measurement of W and Z production cross sections at the CERN $\bar{p}p$ collider, submitted to Z. Phys. C.
[11] F.A. Berends and R. Kleiss, Z. Phys. C 27 (1985) 365.
[12] M. Diemoz, F. Ferroni, E. Longo and G. Martinelli, Z. Phys. C 39 (1988) 21.
[13] G. Altarelli, R.K. Ellis, M. Greco and G. Martinelli, Nucl. Phys. B 246 (1984) 12;
G. Altarelli, R.K. Ellis and G. Martinelli, Z. Phys. C 27 (1985) 617.
[14] UA2 Collab., J. Alitti et al., Measurement of the transverse momentum distributions of W and Z bosons at the CERN $\bar{p}p$ collider, in preparation for Z. Phys. C.
[15] F.A. Berends, Z physics at LEP 1, Vol. 1, CERN Yellow Book CERN 89-08, p. 89.
[16] A.D. Martin, R.G. Roberts and W.J. Stirling, Mod. Phys. Lett. A 4 (1989) 1135.
[17] E. Eichten, I. Hinchliffe, K. Lane and C. Quigg, Rev. Mod. Phys. 56 (1984) 579; 58 (1986) 1065(E).
[18] D.W. Duke and J.F. Owens, Phys. Rev. D 30 (1984) 49.
[19] W.J. Stirling and A.D. Martin, Phys. Lett. B 237 (1990) 551.
[20] A. Sirlin, Phys. Rev. D 22 (1980) 971.
[21] W.J. Marciano and A. Sirlin, Phys. Rev. D 29 (1984) 945.
[22] Particle Data Group, G.P. Yost et al., Review of particle properties, Phys. Lett. B 204 (1988) 51.
[23] W. Hollik and G. Burgers, Z physics at LEP 1, Vol., CERN Yellow Book CERN 89-08.
[24] M. Veltman, Nucl. Phys. B 123 (1977) 89.
[25] ALEPH Collab., D. Decamp et al., CERN preprint CERN-EP/90-16;
OPAL Collab., M.Z. Akrawy et al., Phys. Lett. B 236 (1990) 224.
[26] G.L. Fogli and D. Haidt, Z. Phys. C 40 (1988) 379.